AIP | Applied Physics Letters

Design of three-well indirect pumping terahertz quantum cascade lasers for high optical gain based on nonequilibrium Green's function analysis

Tao Liu, Tillmann Kubis, Qi Jie Wang, and Gerhard Klimeck

Citation: Appl. Phys. Lett. **100**, 122110 (2012); doi: 10.1063/1.3697674
View online: http://dx.doi.org/10.1063/1.3697674
View Table of Contents: http://apl.aip.org/resource/1/APPLAB/v100/i12
Published by the American Institute of Physics.

Design of three-well indirect pumping terahertz quantum cascade lasers for high optical gain based on nonequilibrium Green's function analysis

Tao Liu,[1] Tillmann Kubis,[2] Qi Jie Wang,[1,3,a)] and Gerhard Klimeck[2]
[1]*Division of Microelectronics, School of Electrical & Electronic Engineering, Nanyang Technological University, 50 Nanyang Ave., Singapore 639798*
[2]*Network for Computational Nanotechnology, Birck Nanotechnology Center, Purdue University, West Lafayette, Indiana 47907, USA*
[3]*Division of Physics and Applied Physics, School of Physical and Mathematical Sciences, Nanyang Technological University, Singapore 637371*

(Received 26 November 2011; accepted 5 March 2012; published online 23 March 2012)

The nonequilibrium Green's function approach is applied to the design of three-well indirect pumping terahertz (THz) quantum cascade lasers (QCLs) based on a resonant phonon depopulation scheme. The effects of the anticrossing of the injector states and the dipole matrix element of the laser levels on the optical gain of THz QCLs are studied. The results show that a design that results in a more pronounced anticrossing of the injector states will achieve a higher optical gain in the indirect pumping scheme compared to the traditional resonant-tunneling injection scheme. This offers in general a more efficient coherent resonant-tunneling transport of electrons in the indirect pumping scheme. It is also shown that, for operating temperatures below 200 K and low lasing frequencies, larger dipole matrix elements, i.e., vertical optical transitions, offer a higher optical gain. In contrast, in the case of high lasing frequencies, smaller dipole matrix elements, i.e., diagonal optical transitions are better for achieving a higher optical gain. © *2012 American Institute of Physics*. [http://dx.doi.org/10.1063/1.3697674]

Terahertz (THz) quantum cascade lasers (QCLs) are one of the most important sources of coherent THz radiation. Up to now, they can cover a spectral range from ~1.2 to ~5 THz.[1] Since their invention in 2002,[2] many efforts have been made to improve the THz QCL design to increase their maximum lasing temperature (to increase the optical gain) to the realm of thermo-electric cooling. The state-of-the-art maximum operating temperature of 186 K (Ref. 3) was achieved in a QCL active region design such that electrons are injected into the upper laser levels by resonant tunneling and interwell optical transitions (so-called diagonal design) are used. Since in THz QCLs, the energy separation between the upper and the lower laser levels is relatively small (~4–20 meV), it is difficult to selectively inject electrons only into the upper laser level. Therefore, the injector barrier in resonant-tunneling injection QCLs is relatively thick so that off-resonant tunneling into states other than the upper laser level is suppressed. Typically, the width of the injector barrier is chosen such that the anti-crossing splitting of the injection state and the upper laser level $2\hbar\Omega_{iu}$ (Ω_{iu} is the Rabi frequency of the coupled levels) is smaller than $\hbar\Delta\nu_{scatt}$, i.e., the FWHM linewidth due to scattering.[4] The disadvantage of a small Ω_{iu} and consequently a weak coupling between the injector and the upper laser level is the inefficient injection of electrons into the upper laser level. This effectively limits the dynamic range of THz QCLs, and the maximum achievable optical gain. Based on this resonant-tunneling injection scheme, the maximum operating temperature of THz QCLs turned out to be limited by an empirical relation $T_{\max} \sim \hbar\omega/\kappa_B$ (ω is the laser frequency, κ_B is the Boltzmann constant).[1,5] The indirect pumping scheme has recently managed to surpass this empirical limit.[6–9] Such indirect pumping scheme can be traced back as early as in 2001 by Scamarcio *et al.*[10] In this scheme, as shown in Fig. 1, electrons are injected into the upper laser level (energy state 4) by resonantly emitting phonons from the injector level (energy state 5). In this case, off resonant tunneling from the injector level to the lower laser level is well suppressed. Therefore, it is expected that the injector barriers can be kept thinner than those in the resonant injection scheme, since a pronounced tunneling through the injector barrier does not broaden the laser transition. The indirect pumping scheme may therefore

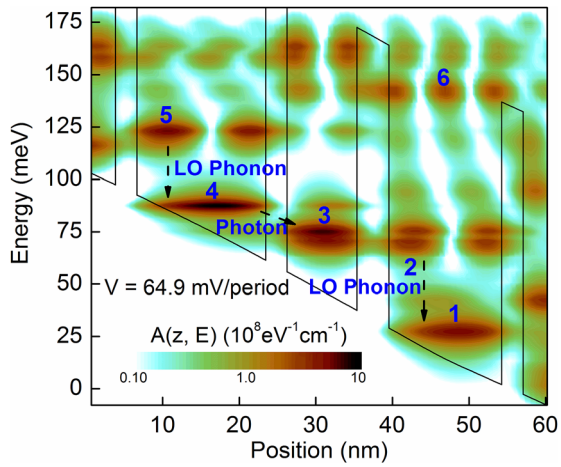

FIG. 1. Contour plot of the energy and spatially resolved spectral function *A(z, E)* of three-well indirect pumping THz QCL as a function of position and energy. The zero in energy marks the chemical potential of the right lead. The applied bias voltage is 64.9 mV per period. The solid line indicates the self-consistent potential profile. The spectral function is only shown in the energy interval from −7 to 180 meV.

a)Electronic mail: qjwang@ntu.edu.sg.

TABLE I. The parameters of the active regions for various anticrossing energy separations of the injector states and laser frequencies. The layer thicknesses start with the injection barrier. All layer thicknesses are given in Angstrom, and bold numbers indicate barriers of $Al_{0.15}Ga_{0.85}As$. The last GaAs wells are doped with a sheet density of $3 \times 10^{10}\,cm^{-2}$ in their central regions.

Lasing frequency	Anticrossing energy separation of the injector states				
	5.10 meV	5.53 meV	6.02 meV	6.50 meV	7.14 meV
3.2 THz	**32**/164/**27**/91/**43**/146	**30**/165/**27**/91/**43**/146	**28**/166/**27**/90/**42**/146	**26**/166/**27**/90/**42**/147	**24**/167/**30**/92/**42**/145
Lasing frequency	Anticrossing energy separation of the injector states				
	5.10 meV	5.59 meV	6.10 meV	6.34 meV	6.61 meV
3.6 THz	**32**/162/**25**/91/**43**/146	**30**/162/**25**/91/**43**/145	**28**/162/**26**/92/**43**/144	**27**/162/**25**/92/**43**/144	**26**/163/**26**/92/**43**/144
Lasing frequency	Anticrossing energy separation of the injector states				
	5.54 meV	6.10 meV	6.45 meV	6.63 meV	7.02 meV
4.0 THz	**30**/157/**20**/91/**43**/144	**28**/157/**20**/90/**43**/143	**26**/157/**20**/90/**43**/144	**26**/157/**20**/9043/142	**25**/158/**20**/90/**43**/141

offer a venue for high-performance THz QCLs. So far, only five and four-well THz QCL designs have been studied.[7,8] While, due to the smaller number of interfaces per period, it is expected that a three-well structure can achieve a higher optical gain and therefore a higher temperature performance. This was evidenced by the fact that three-well THz QCLs based on the resonant tunneling scheme achieved the highest temperature operation.[3]

This Letter proposes and analyzes a set of three-well THz QCLs based on the indirect pumping scheme. The optical gain as functions of the anti-crossing energy separation (i.e., coupling) between the injection states, and the optical dipole matrix element are carefully assessed with the self-consistent non-equilibrium Green's function (NEGF) method. The NEGF method is well known that can be used to accurately investigate incoherent quantum transport in THz QCLs.[11–14] This work uses a real space representation and QCLs are considered as open quantum systems that are connected to dissipative periodic leads.[11] All electrons enter the QCL devices in equilibrium distributions and nonequilibrium electrons that leave the device are thermalized within the leads. Incoherent electron scattering on acoustic phonons, polar optical phonons, charged impurities, and rough interfaces is taken into account within the self-consistent Born approximation.[15–17] The electron-electron interaction is included in the mean-field Hartree approximation. More details of the NEGF model can be found in Ref. 11.

The layer thicknesses of all considered GaAs/$Al_{0.15}Ga_{0.85}As$ THz QCLs and their respective predicted laser frequencies are listed in Table I. The optical gain of THz QCLs depends critically on how strong the coupling of the injection states is designed. To guarantee comparability of the lasers, the coupling strength between the extraction state and the lower laser level (Ω_{ext}) as well as the radiative optical dipole matrix element (z) of all lasers in Table I are kept constant at each designed frequency. Figure 2 shows the calculated maximum local optical gain as a function of the anti-crossing energy separation of the injector states when the lattice temperature is set to 40 and 180 K, respectively. As shown in Fig. 2, the optical gain has a maximum value at an energy separation between the injector states of ~6 meV for all the three emission frequencies at both 40 and 180 K. It is worth to note that the maximum local optical gain of the indirect pumped THz QCLs of Fig. 2 are higher than typical values calculated in resonant tunneling THz-QCLs,[7,18] because electrons of the injector level are more selectively injected into the upper laser level; hence, the parasitic injection into the lower laser level is better suppressed in the indirect pumping design than in the resonant tunneling design.[8] Therefore, the injection anticrossing energy separation can be designed larger in the indirect pumping design (~6 meV) than in the resonant-tunneling injection scheme (~1–2 meV), thus offering a more efficient electron transport. As shown in Fig. 2, the optical gain first increases with the increase of the anticrossing energy separation between the injector states and then decreases. This is because, at the lower injection anti-crossing energy separation side

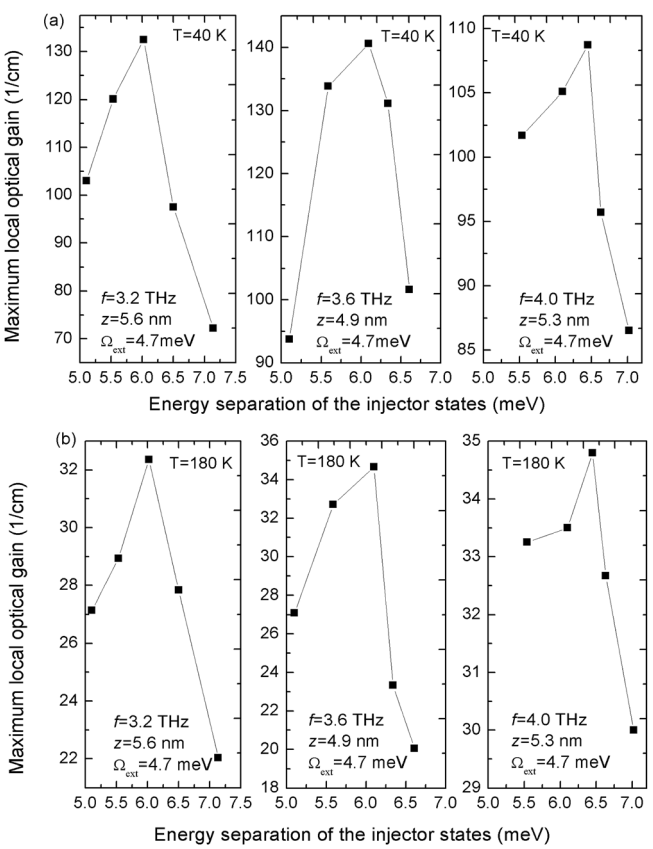

FIG. 2. Calculated maximum local optical gain as a function of the anti-crossing energy separation of the injector states at (a) 40 K and (b) 180 K. The anticrossing energy separation between the extraction state and the lower laser level as well as the optical dipole matrix elements of these designs are kept constant at each designed frequency. Lines are meant to guide the eye.

TABLE II. Parameters of the active regions for various optical dipole matrix elements and laser frequencies. The layer thicknesses start with the injection barrier. All layer thicknesses are given in Angstrom and bold numbers indicate barriers of $Al_{0.15}Ga_{0.85}As$. The last GaAs wells are doped with a sheet density of $3 \times 10^{10}\,cm^{-2}$ in their central regions.

Lasing frequency		Optical dipole matrix element	
	3.93 nm	4.91 nm	5.64 nm
3.2 THz	**28**/167/**36**/93/**43**/145	**28**/166/**31**/92/**43**/145	**28**/166/**27**/90/**42**/146
Lasing frequency		Optical dipole matrix element	
	3.73 nm	4.74 nm	5.95 nm
3.6 THz	**24**/181/**31**/108/**37**/161	**30**/161/**27**/91/**44**/144	**30**/161/**25**/91/**44**/144
Lasing frequency		Optical dipole matrix element	
	3.79 nm	4.81 nm	5.59 nm
4.4 THz	**32**/154/**25**//93/**45**/141	**33**/153/**20**/91/**44**/142	**33**/152/**15**/87/**42**/143

(<6 meV), increasing the coupling of the injector states will increase the amount of electrons that coherently tunnel through the injector barrier and scatter into the upper laser level. While, at the higher injection anti-crossing energy separation side (>6 meV), the coupling of the injector states becomes so strong that the electron leakage into the higher energy state 6 (see Fig. 1) increases. These leakage electrons can scatter non-radiatively into the lower laser level 3 through emitting LO-phonons and thus reduce the population inversion. Furthermore, the reduction of the calculated gain with the increase of the temperature (see Fig. 2(b)) is due to the thermally activated LO phonon scattering from the upper laser level to the lower laser level.[1,7]

The optical dipole matrix element between the upper and the lower laser levels also determines the maximum local optical gain. The indirect pump THz QCLs (see Table II) have been designed to have equal injection (Ω_{inj}) and extraction (Ω_{ext}) anticrossing energy separations at each designed frequency, but different optical matrix elements. Figure 3 shows the calculated maximum local optical gain as a function of the optical dipole matrix element for various lasing frequencies and lattice temperatures. As seen in Figs. 3(a) and 3(b), for lower lasing frequencies at 3.2 and 3.6 THz, a larger dipole matrix element gives a higher optical gain. Instead, for higher lasing frequency at 4.4 THz, as shown in Fig. 3(c), a smaller dipole matrix element induces a higher local optical gain. The reason for this is that the thermally activated LO phonon scattering from the upper laser level to the lower laser level is more prominent at higher lasing frequencies[14] similar to that in resonant tunneling injection THz QCLs.[19,20] Thermally activated LO phonon scattering, however, is better suppressed in the case of smaller spatial overlap of the wavefunctions, i.e., in the diagonal design where the optical dipole matrix element is smaller. In contrast, at the low lasing frequencies, the thermally activated LO phonon scattering does not limit the QCL performance for temperatures below 200 K, which yields the different behavior.[20]

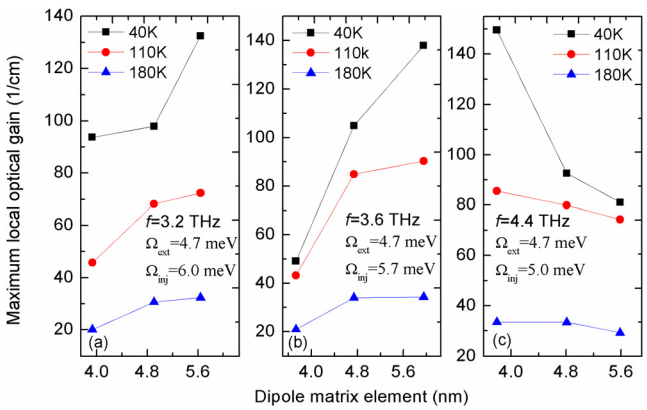

FIG. 3. The calculated maximum local optical gain as a function of the optical dipole element at different lasing frequencies. The anticrossing energy separation between the injector states and between the lower laser level and the extraction state are constant at each designed frequency. Lines are meant to guide the eye.

In conclusion, the NEGF method is applied to predict the performance of three-quantum-well THz QCLs based on the indirect pumping scheme. The influence of the energy separation of the injection states and of the radiative dipole matrix elements on the maximum local optical gain is analyzed. The results show that the indirect pumping scheme, with a larger injection anticrossing energy separation (~6 meV), can have a higher optical gain than the resonant-tunneling injection scheme at both low and high temperatures. For low lasing frequencies, larger local optical gain is achieved with larger dipole matrix elements. Whereas for high lasing frequencies, smaller radiative dipole matrix elements suppress thermally activated LO-phonon scattering and therefore yield higher local optical gain.

We would like to acknowledge the financial support by the grant (Grant No. M58040017) from Nanyang Technological University (NTU), Singapore. Support from the CNRS International-NTU-Thales Research Alliance (CINTRA) Laboratory, UMI 3288, Singapore 637553, is also acknowledged. The nanoHUB.org computational resources operated by the Network for Computational Nanotechnology funded by NSF under EEC-0228390 and OCI-0749140 are utilized in this work and gratefully acknowledged.

[1]B. S. Williams, Nature Photon. **1**, 517 (2007).
[2]R. Kohler, A. Tredicucci, F. Beltram, H. E. Beere, E. H. Linfield, A. G. Davies, D. A. Ritchie, R. C. Iotti, and F. Rossi, Nature (London) **417**, 156 (2002).
[3]S. Kumar, Q. Hu, and J. L. Reno, Appl. Phys. Lett. **94**, 131105 (2009).
[4]S. Kumar and Q. Hu, Phys. Rev. B **80**, 245316 (2009).
[5]M. Belkin, Q. J. Wang, C. Pflugl, A. Belyanin, S. P. Khanna, A. G. Davies, E. H. Linfield, and F. Capasso, IEEE Trans J. Select Quantum Electron. **15**, 952 (2009).
[6]M. Yamanishi, K. Fujita, T. Edamura, and H. Kan, Opt. Express **16**, 20748 (2008).
[7]H. Yasuda, T. Kubis, P. Vogl, N. Sekine, I. Hosako, and K. Hirakawa, Appl. Phys. Lett. **94**, 151109 (2009).

[8]S. Kumar, C. W. I. Chan, Q. Hu, and J. L. Reno, Nat. Phys. **7**, 166 (2011).
[9]T. Kubis, S. R. Mehrotra, and G. Klimeck, Appl. Phys. Lett. **97**, 261106 (2010).
[10]G. Scamarcio, M. Troccoli, F. Capasso, A. L. Hutchinson, D. L. Sivco, and A. Y. Cho, Electron. Lett. **37**, 295 (2001).
[11]T. Kubis, C. Yeh, P. Vogl, A. Benz, G. Fasching, and C. Deutsch, Phys. Rev. B **79**, 195323 (2009).
[12]S.-C. Lee and A. Wacker, Phys. Rev. B **66**, 245314 (2002).
[13]T. Kubis and P. Vogl, Phys. Rev. B **83**, 195304 (2011).
[14]T. Kubis, S. R. Mehrotra, and G. Klimeck, Appl. Phys. Lett. **97**, 261106 (2010).
[15]R. Lake, G. Klimeck, R. C. Bowen, and D. Jovanovic, J. Appl. Phys. **81**(12), 7845 (1997).
[16]G. Klimeck, R. Lake, and D. K. Blanks, Phys. Rev. B **58**(11), 7279 (1998).
[17]R. Lake, G. Klimeck, R. C. Bowen, C. Fernando, T. Moise, Y. C. Kao, and M. Leng, Superlattices Microstruct. **20**, 279 (1996).
[18]T. Kubis and P. Vogl, Laser Phys. **19**, 762 (2009).
[19]Y. Chassagneux, Q. J. Wang, S. P. Khanna, E. Strupiechonski, J.-R. Coudevylle, E. H. Linfield, A. G. Davies, F. Capasso, M. A. Belkin, and R. Colombelli, IEEE Trans. THz Sci. Tech. **2**, 83 (2012).
[20]A. Matyas, M. A. Belkin, P. Lugli, and C. Jirauschek, Appl. Phys. Lett. **96**, 201110 (2010).